Turbulent Transport due to Kinetic Ballooning Modes in High-Beta Toroidal Plasmas

A. Ishizawa[1], S. Maeyama[2], T.-H. Watanabe[1], H. Sugama[1] and N. Nakajima[1]

[1]National Institute for Fusion Science, Toki, Gifu, 509-5292, Japan
[2]Japan Atomic Energy Agency, Rokkasho, Aomori, 039-3212, Japan

Corresponding Author: ishizawa@nifs.ac.jp

Abstract:

Turbulent transport due to kinetic ballooning modes (KBMs) in high-beta toroidal plasmas is investigated by means of an electromagnetic gyrokinetic model and a newly developed electromagnetic hybrid model consisting of the gyrokinetic equation for ions and fluid equations for electrons. Full gyrokinetic simulation results for Cyclone base case tokamak with $\beta = 2\%$ and $\eta_e = 0$ is quickly and accurately reproduced by the hybrid simulation. Agreement between the hybrid and full kinetic simulations are confirmed on detailed transport mechanisms: electrostatic heat and particle fluxes and electromagnetic heat and particle pinches for ions and electrons. The numerical solutions satisfy the entropy balance equation, and entropy variable is transferred from ions to electrons through electromagnetic perturbation. The hybrid model enables us to simulate KBM turbulence in high-beta Large Helical Device (LHD) plasmas, for which full gyrokinetic simulation is difficult because of large computational cost. The critical beta of KBM in the standard LHD plasma is about 1.5% (1%) for $\eta_e = 0$ ($\eta_e = 3$).

1 Introduction

In high-beta torus plasmas micro-turbulence due to kinetic ballooning modes (KBMs) causes anomalous transport of heat and particles, while the growth rate of ion temperature gradient (ITG) instability is suppressed by magnetic field line bending as plasma beta increases [1], where plasma beta β is the normalized plasma pressure. Ballooning modes are related to the degradation of confinement in many torus plasma experiments such as the Large Helical Device (LHD) experiments [2]. The β scaling of turbulent transport is one of the central issues in fusion plasma research. In order to understand the scaling the impact of magnetic perturbation on heat transport through affecting the balance between zonal flow and micro-turbulence should be understood. In addition the validity of Rechester-Rosenbluth model describing direct effects of magnetic perturbation on heat transport is another important issue.

Two of authors studied KBM driven turbulent transport and found the profile stiffness of externally heated tokamak plasmas by means of global two-fluid simulations [3]. In order to investigate electromagnetic turbulent transport more quantitatively, we need to include kinetic effects. Gyrokinetic simulations including both kinetic ions and electrons are applied to the studies of turbulence in finite-beta plasmas [4, 5, 6].

In this work, we investigate electromagnetic turbulent transport in high-beta tokamak and LHD plasmas by means of newly developed simulation codes: GKV+/EM solving gyrokinetic ion and electron equations and GKV+/EMH solving gyrokinetic ion and fluid electron equations. The code is developed by extending GKV [7] that solves gyrokinetic equations with adiabatic electrons.

2 Simulation model

2.1 Electromagnetic gyrokinetic equations

Micro-turbulence in a radially localized flux tube plasma along magnetic field line is investigated. Temperature and density gradients are uniform and direct to x-axis, and temperature gradient is represented by the parameter $\eta_s = L_n/L_{T_s}$ in terms of density scale length $L_n = -(d\ln n/dx)^{-1}$ and temperature scale lengths $L_{Ts} = -(d\ln T_s/dx)^{-1}$, where the subscript s denotes particle spices. The distribution functions are divided into the Maxwellian part and a perturbed part, $F_s = F_{Ms} + \delta f_s$, where $F_{Ms} = \frac{n_0}{(2\pi T_s/m_s)^{3/2}}\exp(-\frac{m_s v_\parallel^2}{2T_s} - \frac{\mu B}{T_s})$, and the perturbed part is represented by $\delta f_s = \sum_k \delta f_{sk}\exp(iS_k)$, where $\nabla S_k = \mathbf{k}_\perp$. The model consists of the gyrokinetic equation of perturbed part of distribution functions,

$$\frac{D\delta f_{sk}}{\partial t} + v_\parallel \mathbf{b}^*\cdot\nabla\delta f_{sk} = -i\mathbf{v}_{ds}\cdot\mathbf{k}_\perp(\delta f_{sk} + \frac{q_s}{T_s}F_{Ms}\phi_k J_{0s}) - v_\parallel\frac{q_s}{T_s}F_{Ms}E_{\parallel k}J_{0s} + \frac{\mu}{m_s}\mathbf{b}\cdot\nabla B\frac{\partial\delta f_{sk}}{\partial v_\parallel} + i\mathbf{v}_{*s}\cdot\mathbf{k}_\perp\frac{q_s}{T_s}F_{Ms}(\phi_k - \frac{v_\parallel}{c}A_{\parallel k})J_{0s} + C_s(\delta f_{sk}), \quad (1)$$

the gyrokinetic Poisson and Ampere's equations,

$$k_\perp^2\phi_k = 4\pi\sum_s q_s(\delta n_{sk} - \frac{q_s n_0}{T_s}(1-\Gamma_{0s})\phi_k), \qquad k_\perp^2 A_{\parallel k} = \frac{4\pi}{c}\sum_s q_s n_0\delta u_{sk}, \quad (2)$$

where $E_{\parallel k} = -\mathbf{b}^*\cdot\nabla\phi_k - \frac{1}{c}\frac{\partial A_{\parallel k}}{\partial t}$, $\delta n_{sk} = \int\delta f_{sk}J_{0s}d^3v$, $n_0\delta u_{sk} = \int v_\parallel\delta f_{sk}J_{0s}d^3v$, $q_i = e$, $q_e = -e$. In Eq. (1) $\frac{Df_k}{Dt} = \frac{\partial f_k}{\partial t} + \frac{c}{B}[\phi J_{0s}, f]_k$ and $\mathbf{b}^*\cdot\nabla f_k = \mathbf{b}\cdot\nabla f_k - \frac{1}{B}[A_\parallel J_{0s}, f]_k$, where $[f,g]_k = \sum_{k',k''}\delta_{k,k'+k''}\mathbf{b}\cdot\mathbf{k}'_\perp\times\mathbf{k}''_\perp f_{k'}g_{k''}$. The drift velocities are $\mathbf{v}_{ds} = \frac{c}{q_s B}\mathbf{b}\times(\mu\nabla B + m_s v_\parallel^2\mathbf{b}\cdot\nabla\mathbf{b})$ and $\mathbf{v}_{*s} = \frac{cT_s}{q_s B}\mathbf{b}\times\nabla\ln F_{Ms}$, and $C_s(\delta f_{sk})$ is the Lenard-Bernstein collision operator. In Eq. (2) $\Gamma_{0s} = e^{-b_{sk}}I_0(b_{sk})$ and $b_{sk} = \rho_s^2 k_\perp^2$, where I_0 are the zeroth order modified Bessel function.

The entropy balance equation is obtained from Eqs. (1)-(2) [8] and is written as

$$\frac{d}{dt}\left(\sum_s\delta S_s + W_{es} + W_{em}\right) = \frac{Q_{es,s}+Q_{em,s}}{L_{Ts}} + \frac{T_s(\Gamma_{es,s}+\Gamma_{em,s})}{L_{ps}} + D_s, \quad (3)$$

where $\delta S_s = \left\langle \sum_k \int d^3v \frac{T_s |\delta f_{sk}|^2}{2F_{sM}} \right\rangle$, $D_s = \left\langle \sum_k \int d^3v \frac{T_s \delta f_{sk}^* C_s}{F_{sM}} \right\rangle$,
$W_{es} = \left\langle \sum_k \left(\frac{k_\perp^2}{4\pi} + \frac{n_0 q_s^2}{T_s}[1 - \Gamma_0(b_{sk})] \right) \frac{|\delta\phi_k|^2}{2} \right\rangle$, $W_{em} = \left\langle \sum_k \frac{k_\perp^2}{4\pi} \frac{|A_{\parallel k}|^2}{2} \right\rangle$,
$Q_{es,s} = \left\langle Re \left[\sum_k \left(\frac{1}{2}\delta p_{\parallel s} + \delta p_{\perp s} - \frac{5}{2} T_s \delta n_s \right) \left(\frac{-ik_y \phi_k c}{B} \right)^* \right] \right\rangle$,
$Q_{em,s} = \left\langle Re \left[\sum_k \left(\frac{1}{2}\delta q_{\parallel s} + \delta q_{\perp s} \right) \left(\frac{ik_y A_{\parallel k}}{B} \right)^* \right] \right\rangle$,
$\Gamma_{es,s} = \left\langle Re \left[\sum_k \delta n_s \left(\frac{-ik_y \phi_k c}{B} \right)^* \right] \right\rangle$, $\Gamma_{em,s} = \left\langle Re \left[\sum_k n_0 \delta u_s \left(\frac{ik_y A_{\parallel k}}{B} \right)^* \right] \right\rangle$, where $<>$ denotes the flux surface average.

2.2 Electron fluid hybrid model

In order to simulate KBM turbulence efficiently we introduce a new hybrid model of gyrokinetic ions and fluid electrons and have developed GKV+/EMH code. Our new model enables us to simulate KBM at high-beta more quickly than the conventional model with kinetic electrons. The model consists of the gyrokinetic equation of perturbed distribution functions of ions Eq. (1), the gyrokinetic Poisson and Ampere's equations Eq. (2) and a set of moment equations of the electron gyrokinetic equation obtained by assuming the electron Larmor radius is small, $\rho_e k_\perp \ll 1$, so that $J_{0e}(\rho_e \to 0) = 1$. The fluid equations obtained from the moment equations are density, parallel velocity, parallel pressure, $\delta p_{\parallel s} = \int m_s v_\parallel^2 \delta f_s J_{0s} d^3v = n_0 \delta T_{\parallel s} + T_s \delta n_s$, perpendicular pressure $\delta p_{\perp s} = \int \mu B \delta f_s J_{0s} d^3v = n_0 \delta T_{\perp s} + T_s \delta n_s$, parallel heat flux, $n_0 \delta q_{\parallel s} = \int m_s v_\parallel^3 \delta f_s J_{0s} d^3v - 3 n_0 T_s \delta u_s$, and perpendicular heat flux $n_0 \delta q_{\perp s} = \int \mu B v_\parallel \delta f_s J_{0s} d^3v - n_0 T_s \delta u_s$, equations [9, 10],

$$\frac{D\delta n_{ek}}{Dt} + n_0 B \mathbf{b}^* \cdot \nabla \frac{\delta u_{ek}}{B} = -i \mathbf{v}_{def} \cdot \mathbf{k}_\perp \frac{\delta p_{\parallel e} + \delta p_{\perp ek} + 2 q_e n_0 \phi_k}{T_e} - i \mathbf{v}_{*ef} \cdot \mathbf{k}_\perp n_0 \frac{q_e \phi_k}{T_e} \quad (4)$$

$$-\frac{q_e n_0}{c} \frac{\partial A_{\parallel k}}{\partial t} = q_e n_0 \mathbf{b}^* \cdot \nabla \phi_k + \mathbf{b}^* \cdot \nabla \delta p_{\parallel ek} + (\delta p_{\parallel ek} - \delta p_{\perp ek}) \mathbf{b} \cdot \nabla \ln B + \frac{q_e n_0}{c} i(1 + \eta_e) \mathbf{v}_{*ef} \cdot \mathbf{k}_\perp A_{\parallel k} - i m_e \frac{n_0}{T_e} \mathbf{v}_{def} \cdot \mathbf{k}_\perp (\delta q_{\parallel e} + \delta q_{\perp ek} + 4 q_e T_e \delta u_{ek}), \quad (5)$$

$$n_0 \frac{D\delta T_{\parallel ek}}{Dt} + n_0 T_e B \mathbf{b}^* \cdot \nabla \frac{2\delta u_{ek}}{B} + n_0 B \mathbf{b} \cdot \nabla \frac{\delta q_{\parallel ek}}{B} = i 2 \eta_e \mathbf{v}_{*ef} \cdot \mathbf{k}_\perp q_e n_0 \phi_k - i \mathbf{v}_{de} \cdot \mathbf{k}_\perp (4 n_0 \delta T_{\parallel ek} + 2 \delta p_{\parallel ek} + 2 q_e n_0 \phi_k) - 2 n_0 (q_{\perp ek} + T_e \delta u_{ek}) \mathbf{b} \cdot \nabla \ln B, \quad (6)$$

$$n_0 \frac{D\delta T_{\perp ek}}{Dt} + n_0 B \mathbf{b} \cdot \nabla \frac{\delta q_{\perp ek}}{B} = -i q_e n_0 \eta_e \mathbf{v}_{*ef} \cdot \mathbf{k}_\perp \phi_k - i \mathbf{v}_{def} \cdot \mathbf{k}_\perp (3 n_0 \delta T_{\perp e} + \delta p_{\perp ek} + q_e n_0 \phi_k) + n_0 (q_{\perp ek} + T_e \delta u_e) \mathbf{b} \cdot \nabla \ln B, \quad (7)$$

$$\frac{D\delta q_{\parallel ek}}{Dt} + (3 + \beta_\parallel) \frac{T_e}{m_e} \mathbf{b} \cdot \nabla \delta T_{\parallel ek} = -i \mathbf{v}_{def} \cdot \mathbf{k}_\perp (3 \delta q_{\parallel ek} - 3 \delta q_{\perp ek} - \alpha_\parallel n_0 T_e \delta u_{ek}) - 3i \frac{q_e T_e}{m_e c} \eta_e \mathbf{v}_{*ef} \cdot \mathbf{k}_\perp A_{\parallel k} - \sqrt{2} v_{Te} \frac{D_\parallel}{q_0 R} \delta q_{\parallel ek} + \mu_e \nabla_\perp^2 \delta q_{\parallel ek}, \quad (8)$$

$$\frac{D\delta q_{\perp ek}}{Dt} + \frac{T_e}{m_e} \mathbf{b} \cdot \nabla \delta T_{\perp ek} = -\frac{q_e T_e}{m_e c} i \eta_e \mathbf{v}_{*ef} \cdot \mathbf{k}_\perp A_{\parallel k} + \frac{T_e}{n_0 m_e} (\delta p_{\parallel ek} - \delta p_{\perp ek}) \mathbf{b} \cdot \nabla \ln B - i \mathbf{v}_{def} \cdot \mathbf{k}_\perp (-\delta q_{\parallel ek} - \delta q_{\perp ek} + n_0 T_e \delta u_{ek}) - \sqrt{2} v_{Te} \frac{D_\perp}{q_0 R} \delta q_{\perp ek} + \mu_e \nabla_\perp^2 \delta q_{\perp ek}, \quad (9)$$

where the parameters are set to be $\beta_\parallel = -3/2$ and $\alpha_\parallel = 3$, so that the model is consistent with the entropy balance equation. The electron inertia terms in Eq. (5) are neglected by assuming small mass-ratio $m_e/m_i \ll 1$. In the hybrid model δS_e and D_e in the entropy balance equation Eq. (3) are replaced to $\delta S_e = \left\langle \sum_k \frac{n_0 T_e}{2} \left(\frac{|\delta n_{ek}|^2}{n_0^2} + \frac{|\delta T_{\parallel ek}|^2}{2T_e^2} + \frac{|\delta T_{\perp ek}|^2}{T_e^2} + \frac{1}{3} \frac{|\delta q_{\parallel ek}|^2}{T_e^3/m_e} + \frac{|\delta q_{\perp ek}|^2}{T_e^3/m_e} \right) \right.$ and $D_e = - \left\langle \sum_k k_\perp^2 \frac{n_0 m_e}{T_e^2} \left(\left(\frac{\mu_e}{3} + \sqrt{2} \frac{v_{Te}}{q_0 R} D_\parallel \right) |\delta q_{\parallel ek}|^2 + \left(\mu_e + \sqrt{2} \frac{v_{Te}}{q_0 R} D_\perp \right) |\delta q_{\perp ek}|^2 \right) \right\rangle$.

3 Numerical results

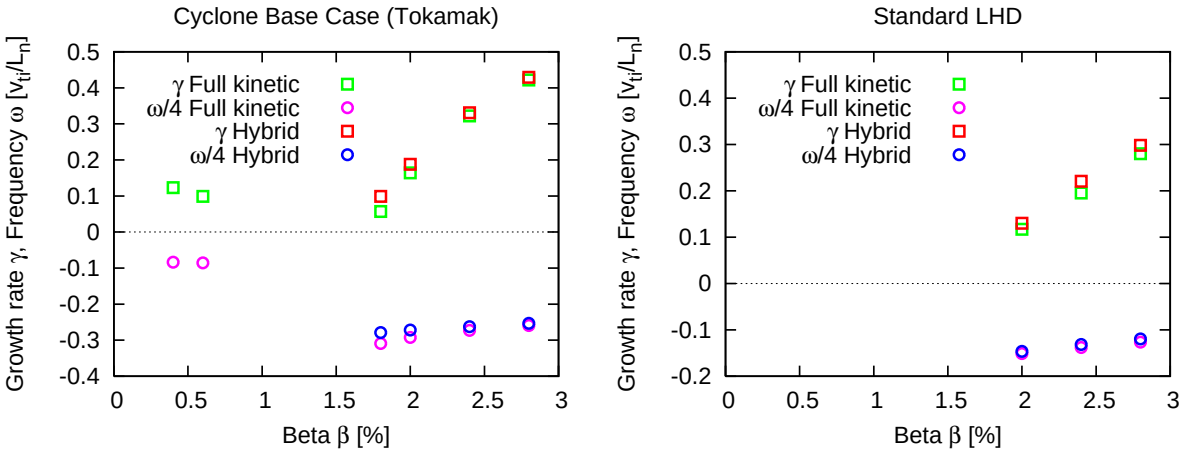

Figure 1: Growth rates and real frequencies as a function of beta for the CBC tokamak with $\eta_e = 0$ and $k_y \rho_i = 0.2$ (left) and for the standard LHD with $\eta_e = 0$ and $k_y \rho_i = 0.19$ (right). Results by the full kinetic and the hybrid calculations are in good agreement for kinetic ballooning modes which appear at high-beta regime.

By extending the gyrokinetic simulation code GKV+, which is electrostatic and adopts adiabatic electron response, we have developed GKV+/EM solving the full gyrokinetic equations [11] and GKV+/EMH solving the hybrid equations.

The perpendicular wavenumber and drift frequencies are written in terms of the flux tube coordinate $(x, y, z, v_\parallel, \mu)$, as $k_\perp^2 = (k_x + \hat{s} z k_y)^2 + k_y^2$, $\mathbf{v}_{ds} \cdot \mathbf{k}_\perp / v_{ds} = \mathbf{v}_{dsf} \cdot \mathbf{k}_\perp / v_{dsf} = (k_x \sin z + k_y (\cos z + \hat{s} z \sin z))$, $\mathbf{v}_{*s} \cdot \mathbf{k}_\perp / v_{*s} = \mathbf{v}_{*sf} \cdot \mathbf{k}_\perp / v_{*sf} = k_y$, where $v_{ds} = v_{dsf}(m_s v_\parallel^2 + \mu B)/T_s$, $v_{*s} = v_{*sf}(1 + (m_s v_\parallel^2/(2T_s) + \mu B/T_s - 3/2)\eta_s)$, $v_{dsf} = \frac{-T_s c}{q_s R_0 B}$, $v_{*sf} = \frac{-T_s c}{q_s L_n B}$. The number of Fourier modes is 288×72. In the z, $v_{\parallel s}$ and μ direction, 64, 64, 16 (256, 64, 16 for the LHD) grid points are uniformly distributed. The collision frequency and the Debye length are set to be $\nu_i = 2 \times 10^{-3}$ and $\lambda_{Di}/\rho_i = 0$, respectively.

Calculations are carried out for the Cyclone base case (CBC) tokamak parameters, $q_0 = 1.4$, $\hat{s} = 0.786$, $\eta_i = 3.1$, $R/L_n = 2.22$, $r_0/R = 0.18$, $T_i = T_e$, except $\eta_e = 0$, and a model configuration of standard LHD experiments $q_0 = 1.9$, $\hat{s} = -0.85$, $\eta_i = 3$, $R/L_n = 3.33$, $r_0/R = 0.11$, $T_i = T_e$, except $\eta_e = 0$ by using the full kinetic code GKV+/EM and the hybrid code GKV+/EMH.

3.1 Linear analysis of finite-beta plasmas

Growth rates and real frequencies as a function of β for $k_y\rho_i = 0.2$ mode are plotted in FIG. 1. The results of CBC tokamak by the full kinetic calculation show the growth rate of ITG instability decreases with β up to $\beta = 1$ %, and then KBM appears, when β is larger than 1.5 %. These KBMs are reproduced by the hybrid calculation. The growth rate of KBM increases with β, while its frequency decreases.

The hybrid model also provide good approximation of growth rates and real frequencies for the LHD plasmas from the full kinetic calculation. The extrapolation of growth rates in FIG. 2 implies that the critical beta of KBM destabilization in the standard LHD is about 1.5% for $\eta_e = 0$ and is about 1% for $\eta_e = 3$. Profiles of electrostatic potential ϕ and parallel component of vector potential $A_\parallel$ in the parallel direction z are also shown in FIG. 2. The oscillation in z direction is caused by the helical magnetic field. These results are qualitatively consistent with the linear analysis of KBMs for LHD [12].

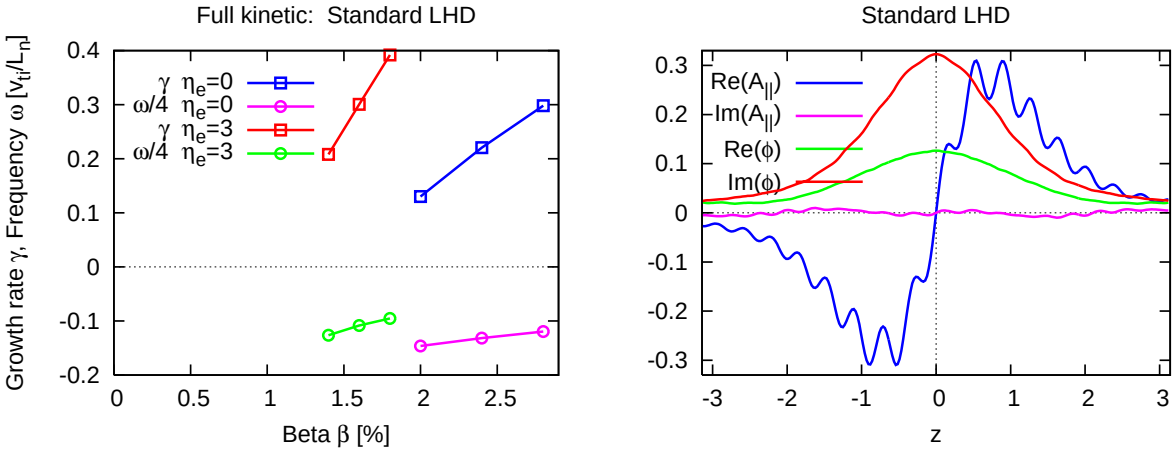

Figure 2: Growth rates and real frequencies of KBMs in the standard LHD from the full kinetic calculation with $\eta_e = 0$ and 3 (left), and profiles of ϕ and $A_\parallel$ of the KBM (right).

3.2 Heat and particle transport in high-beta plasmas

Nonlinear simulations of CBC tokamak and of the standard configuration of LHD with $\beta = 2$ % are carried out. In order to avoid electron temperature gradient instabilities the electron temperature gradient is set to be zero, $\eta_e = 0$ in the simulations. Figure 3 shows time evolution of square of electrostatic potential $< |\phi_k|^2 >$ for each $k_y = 0.05k/\rho_i$ mode. Kinetic ballooning modes grow exponentially at the beginning, and then they get saturated around $t = 50L_n/v_{Ti}$. The amplitude of most unstable mode $k = 5$ (yellow) decreases after it gets saturated, and the $k = 4$ mode (light blue) dominates in the quasi-steady state. The amplitude of zonal flow energy represented by $k = 0$ mode (red line with crosses) is an order of magnitude smaller than the dominant $k = 4$ mode. The weak zonal flow in the KBM turbulence is in contrast with strong zonal flow in ITG turbulence.

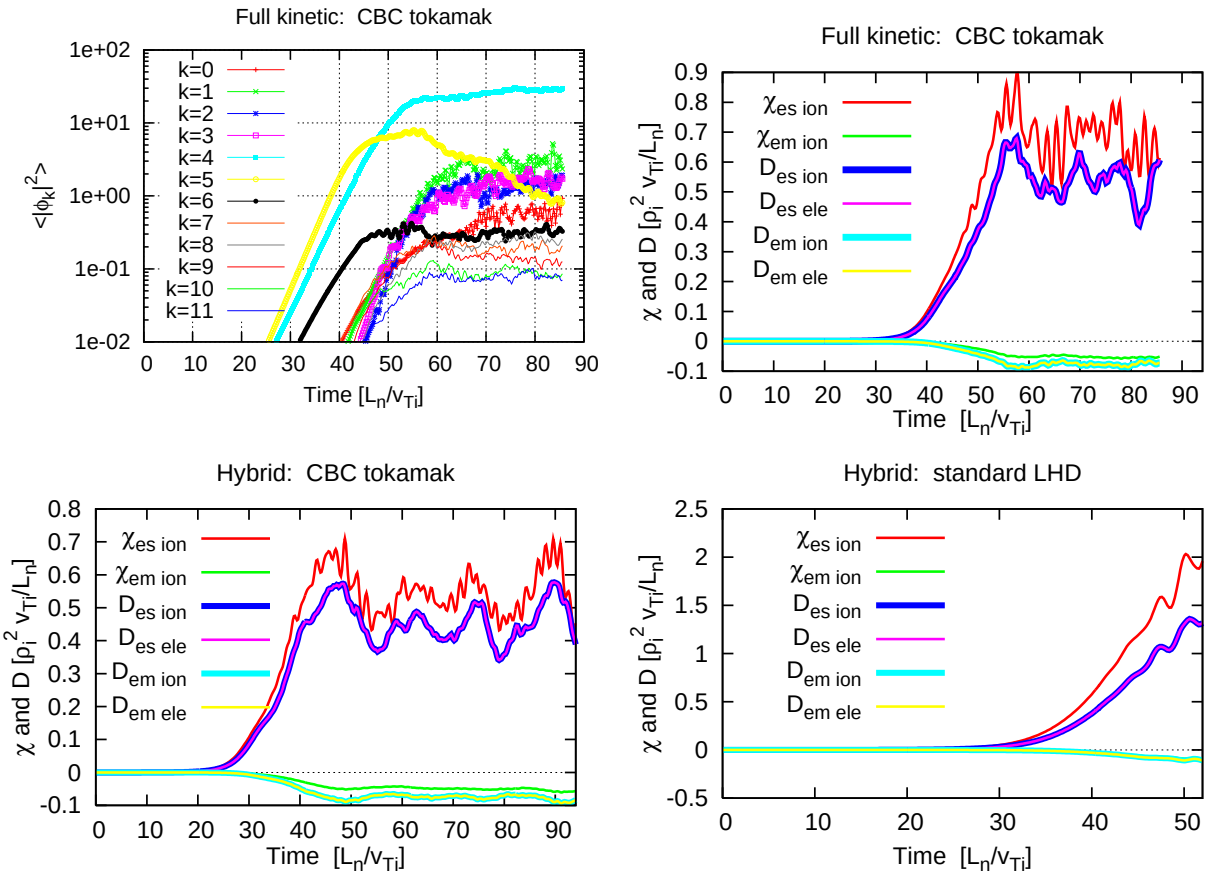

Figure 3: Time evolution of square of electrostatic potential for each k mode $< |\phi_k|^2 >$ (top, left) and of heat and particle transport coefficients, χ and D, of the CBC tokamak by the full kinetic (top, right) and by the hybrid (bottom, left) simulations, and of the standard LHD by the hybrid simulation (bottom, right), with $\eta_e = 0$ and $\beta = 2\%$.

Figure 3 also shows time evolution of heat transport coefficients due to electrostatic (magnetic) perturbation, $\chi_{es,s} = L_{Ts}Q_{es,s}/T_s$ ($\chi_{em,s} = L_{Ts}Q_{em,s}/T_s$) and particle transport coefficients due to electrostatic (magnetic) perturbation, $D_{es,s} = L_{ps}\Gamma_{es,s}/n_0$ ($D_{em,s} = L_{ps}\Gamma_{em,s}/n_0$), where $L_{ps} = L_n/(1+\eta_s)$ and s denotes particle spices. The transport coefficients becomes large as KBMs grow and get saturated around $t = 50L_n/v_{Ti}$ for both of the CBC tokamak and the standard LHD. The ion heat (particle) transport coefficient $\chi_{es,ion}$ ($D_{es,ion}$) is about 0.6 (0.5) $\rho_i^2 v_{Ti}/L_n$ for the tokamak. The ion and electron particle transport caused by electrostatic (magnetic) perturbation are the same, $D_{es,ion} = D_{es,ele}$ and $D_{em,ion} = D_{em,ele}$, because of the quasi-neutrality condition (Ampere's law). The transports due to magnetic perturbation causing magnetic-flutter is much smaller than those by electrostatic perturbation causing radial ExB flow convection. In addition, both of heat and particle transports by magnetic perturbation are negative, and thus the magnetic perturbation of KBM turbulence has pinch effects.

3.3 Entropy balance in finite-beta plasmas

Figure 4 shows time evolution of several groups of terms in the entropy balance equation Eq. (3): the time derivative group $d(S_i + S_e + W_{es} + W_{em})/dt$, the transport group $Q_s/L_T + \Gamma_s T_s/L_{ps}$, and the dissipation group D_s, for the nonlinear simulation of KBM in CBC tokamak. The results by the full kinetic (left) and the hybrid (right) simulations are in good agreement. The numerical error Δ representing difference between the left-hand-side and right-hand-side of Eq. (3) is much smaller than the ion transport group, $Q_i/L_T + \Gamma_i T_i/L_{pi}$, in both simulations. Hence, our numerical results satisfy the entropy balance equation well. The ion transport group is much larger than electron transport group because KBM is unstable in ion-scale. We remark that electron heat transport is zero because $\eta_e = 0$. The small oscillation of the ion transport group is due to the shear Alfven wave and balances with that of the time derivative group. The time derivative group is dominated by dS_i/dt and becomes small after $t = 60$, and then the system reaches a quasi-steady state. In the quasi-steady state the sum of ion heat and particle transport terms, $Q_i/L_T + \Gamma_i T_i/L_{pi}$, almost balances with the sum of ion and electron dissipation terms $D_i + D_e$. On the other hand, the electron transport group, $Q_e/L_T + \Gamma_e T_e/L_{pe}$, does not balance with the electron dissipation term D_e. This implies that the entropy variable is transferred from ions to electrons through electromagnetic potential perturbation and the transferred variable is diffused by the electron dissipation as shown for slab ITG turbulence with $\beta = 0$ in Ref. [13].

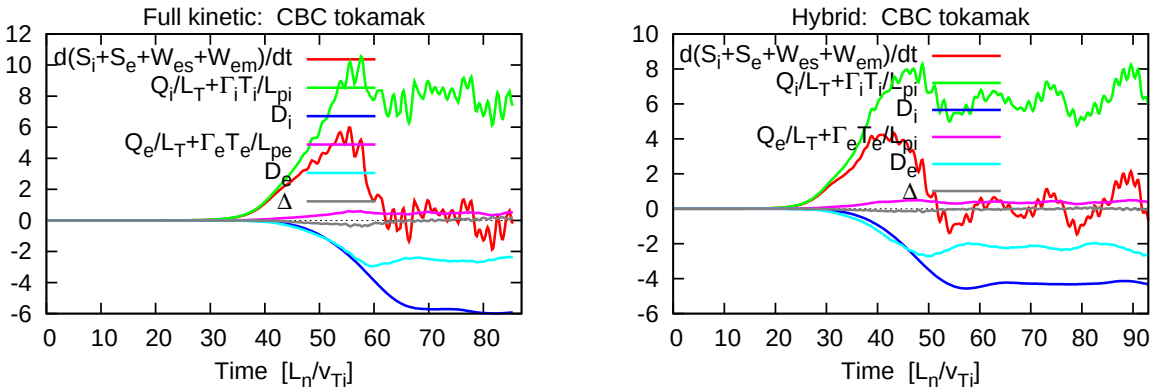

Figure 4: Time evolution of several groups of terms in the entropy balance equation Eq. 3 for the CBC tokamak with $\eta_e = 0$ and $\beta = 2\%$ by the full kinetic (left) and the hybrid (right) simulations. The error Δ representing the difference between the left-hand-side and right-hand-side in the equation is small.

4 Summary

Electromagnetic simulation codes: solving the gyrokinetic ion and electron equations and solving the hybrid model of gyrokinetic ion and fluid electron equations are newly de-

veloped. These codes are applied to the analysis of turbulent transport due to KBM in high-beta CBC tokamak and in a model configuration of standard LHD plasmas. The accuracy of the hybrid model is confirmed by comparing with linear results for the tokamak and LHD plasmas from the full kinetic code. Critical values of KBM onset in the standard LHD configuration are about 1.5% for $\eta_e = 0$ and about 1% for $\eta_e = 3$. In nonlinear calculations the hybrid code is about four times faster than the full kinetic code, and reproduces detailed transport mechanisms. The electrostatic heat (particle) transport coefficient of ion is about 0.6 (0.5) $\rho_i^2 v_{Ti}/L_n$. The magnetic perturbation of KBM turbulence has pinch effects on the heat and particle transport. Turbulent fluctuation of KBM satisfies the entropy balance equation, and the entropy variable is transferred from ions to electrons. The hybrid code enables us to carry out nonlinear simulations of KBM turbulence in high-beta LHD plasmas, for which full gyrokinetic simulation is difficult because of large computational cost, and shows the early stage of nonlinear saturation of KBM at $\beta = 2\%$.

The work is supported by the Japanese Ministry of Education, Culture, Sports, Science and Technology, Grant Nos. 23561003 and 21560861 and by NIFS Collaborative Research Program (NIFS12KNTT015).

References

[1] Kim, J.Y., Horton, W., and Dong, J. Q., Phys. Fluids **B 5**, (1993) 4030.

[2] Ohdachi, S., Tanaka, K., Watanabe, K.Y., et.al., Cont. Plasma Phys. **50**, (2010) 552.

[3] Ishizawa, A. and Nakajima, N., Nuclear Fusion **49**, (2009) 055015.

[4] Candy, J., Phys. Plasmas **12** (2005) 072307.

[5] Pueschel, M.J., Kammerer, M., Jenko, F., Phys. Plasmas **15** (2008) 102310.

[6] Pueschel, M.J., and Jenko, F., Phys. Plasmas **17** (2010) 062307.

[7] Watanabe, T.-H., Sugama, H., Margalet, S.F., Phys. Rev. Lett. **100**, (2008) 195002.

[8] Sugama, H., Watanabe, T.-H., Nunami, M., Phys. Plasmas **16** (2009).

[9] Beer M.A., and Hammett, G.W., Phys. Plasmas 3,(1996) 4046.

[10] Scott, B., Phys. Plasmas 7, 1845 (2000).

[11] Maeyama, S., Ishizawa, A., Watanabe, T.-H., et.al., preparing.

[12] Sugama H. and Watanabe, T.-H., Phys. Plasmas **11**, (2004) 3068.

[13] Ishizawa, A., Watanabe, T.-H., Nakajima, N., Plasma Fusion Res., **6** (2011) 2403087.